# Electrocatalytic Proton Reduction by a Dicobalt Tetrakis-Schiff Base Macrocycle in Nonaqueous Electrolyte

Subhadeep Kal,[†] Alexander S. Filatov,[‡] and Peter H. Dinolfo*,[†]

[†]Department of Chemistry and Chemical Biology, Rensselaer Polytechnic Institute, 110 Eighth Street, Troy, New York 12180, United States

[‡]Department of Chemistry, University at Albany, State University of New York, Albany, New York 12222, United States

S *Supporting Information*

ABSTRACT: A series of dicobalt complexes, Co_2L^{2+} and Co_2LAc^+, where **L** is a N_6O_2 coordinating bis(phenolate) tetrakis-Schiff base ligand, have been synthesized and characterized via electrochemical and spectroscopic techniques. $[Co_2LAc](ClO_4)$ crystallizes in the monoclinic space group $P2_1/n$, and the structure reveals a highly distorted octahedral geometry for the Co^{II} ions, which are bridged by an acetate with a Co−Co distance of 3.2 Å. Cyclic voltammetry (CV) of Co_2L^{2+} and Co_2LAc^+ in anhydrous acetonitrile reveals large anodic/ cathodic peak splitting for the $Co^{II/III}$ redox transitions and a multielectron wave for the $Co^{II/I}$ reductions. The CVs for Co_2L^{2+} and Co_2LAc^+ were also compared to those of Zn_2LAc^+ and H_4L^{2+} to identify the ligand-center oxidations and

reductions. Addition of trifluoroacetic acid (TFA) or acetic acid (AcOH) to the electrolyte solutions of Co_2L^{2+} results in an irreversible reduction wave that is consistent with electrocatalytic H^+ reduction. The catalytic rate law shows a first order dependence on [catalyst] and a second order dependence on [acid]. Using TFA as the acid source, the electrocatalytic H^+ reduction rate constant for Co_2L^{2+} was determined to be 138 M^{-2} s^{-1}, while coordination of acetate slows the rate to 63 M^{-2} s^{-1} for Co_2LAc^+. Controlled potential electrolysis of Co_2L^{2+} with AcOH generated H_2 in 72−94% Faradaic efficiency as determined by gas chromatography. Initial studies suggest Co^I_2 as the catalytically active form of the complex. These complexes represent a new class of Co-based electrocatalytic H^+ reduction catalysts that utilize a bimetallic active site.
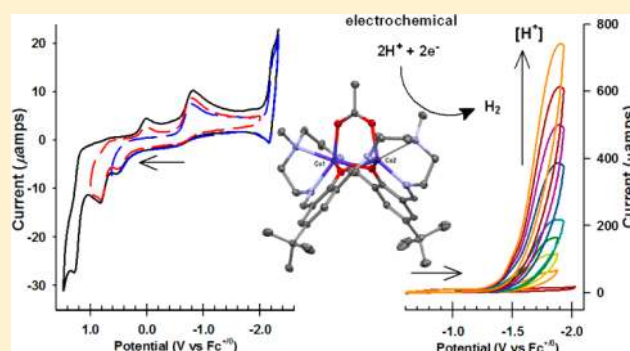
INTRODUCTION

Over the past several decades, significant effort has been focused on the creation of molecular components for artificial photosynthesis systems that use sunlight to drive the splitting of water into O_2 and H_2. The most common approach to creating an artificial photosynthetic device involves the development of efficient and robust catalysts for each half-reaction of water splitting, the oxidation of water to O_2 and reduction of H^+ to H_2.

Recently, there has been increasing interest in developing coordination complexes utilizing first row transition metals in electrocatalysts for H^+ reduction.[1] One such complex that has garnered significant attention from a number of research groups is the mononuclear series of cobaloxime complexes.[2,3] These have been shown to electrocatalytically reduce H^+ to H_2 at relatively low overpotentials and moderate rates with a wide variety of acids.[4] In addition, there have also been studies on photocatalytic H^+ reduction using cobaloxime catalysts.[4−9] Given the number of different research groups working on cobaloxime complexes and the wide range of conditions used to study them, it is not surprising that there is some debate on the mechanism for H^+ reduction to H_2. The three most common mechanistic cycles proposed for H^+ reduction are the

heterolytic pathways of $H^+ + Co^{III}−H \rightarrow H_2 + Co^{III}$,[10−14] or $H^+ + Co^{II}−H \rightarrow H_2 + Co^{II}$,[9,14−18] and the bimolecular homolysis pathway of $2Co^{III}−H \rightarrow H_2 + 2Co^{II}$.[4,8,16,19−21] Several dinuclear nickel, iron, and nickel−iron complexes have been investigated for electrocatalytic H^+ reduction,[22−25] but surprisingly, very few dicobalt. To the best of our knowledge, few such examples have been reported, an octamethylene linked bis(cobaloxime) dimer by Gray et al.,[26] pyridazine based dicobalt complexes by Peters et al.,[27] and bis(pyridyl)pyrazolato bridged di-Co(terpyridine) by Llobet, Fukuzumi, and co-workers.[28] The latter complex has a Co−Co distance of 3.9 Å, and the authors proposed an H^+ reduction mechanism involving the formation of $[Co^{II}Co^{III}−H]$ from $[Co^{II}Co^{I}]$ and H^+, followed by heterolytic attack by a second H^+ to give H_2.

We have become interested in dinuclear tetrakis-Schiff base macrocycles as possible coordination complexes for water splitting reactions. In 1970, Robson showed that the $[2 + 2]$ condensation of 2,6-diformyl-4-phenol with 1,2-diaminopropane can be templated by various first row transition metal dications, including Co(II), to give a dinuclear N_4O_2 Schiff base

macrocycle where the metal centers are approximately 3 Å apart.[29] This method is also somewhat flexible, allowing the incorporation of different aminoalkane side groups, which changes the coordination environment of the two transition metal centers. For example, utilizing *N*-methyl-2,2′-diaminodiethyldiamine provides a N_6O_2 ligation sphere for the two metals, each in a highly distorted octahedral coordination environment.[30−35]

The N_6O_2 ligation sphere of this macrocycle maintains the metal−metal distance at ∼3 Å and also provides two adjacent coordination spots for substrate binding.[30] Based on the reported electrocatalytic H+ reduction activity of other dicobalt complexes mentioned above, we wondered whether a dicobalt tetrakis-Schiff base complex may also display such activity. Herein we describe the electrocatalytic reduction of H^+ by two analogous dicobalt tetrakis-Schiff base complexes, **Co₂LAc⁺** and **Co₂L²⁺**, as H^+ reduction catalysts in acetonitrile (MeCN) using trifluoroacetic acid (TFA) and acetic acid (AcOH) as H^+ sources, where **L** represents the N_6O_2 Schiff base macrocyclic ligand and **Ac** denotes a bridging acetate. To provide a better understanding of the electrochemical and spectroscopic properties of these dicobalt tetrakis-Schiff base complexes, we also compared the analogous zinc and protonated versions of the catalyst, **Zn₂LAc⁺** and **H₄L²⁺**, respectively, which allow us to characterize the contributions from the ligand framework alone.
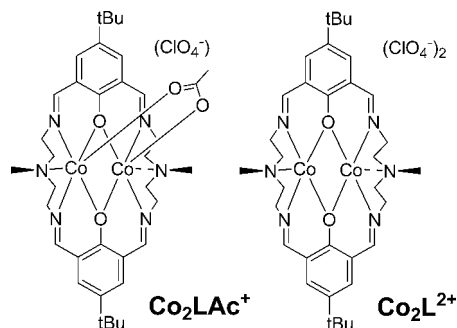
Co₂LAc⁺   **Co₂L²⁺**

RESULTS AND DISCUSSION

Synthesis and Characterization. The syntheses of **Co₂LAc⁺** and **Co₂L²⁺** followed the M^{2+} templated [2 + 2] macrocyclic condensation reaction of Robson and co-workers (Scheme S1 in the Supporting Information).[29,35,36] $Co(ClO_4)_2$, 4-*tert*-butyl-2,6-diformylphenol, and *N*-methyl-2,2′-diaminodiethyldiamine were added to methanol and refluxed under N_2, yielding $[\mathbf{Co_2L}](ClO_4)_2$, where **L** is the bis(phenolate) tetrakis-Schiff base macrocyclic ligand. Addition of one equivalent of sodium acetate to the reaction mixture yields $[\mathbf{Co_2LAc}](ClO_4)$. The completion of the [2 + 2] condensation reactions for **Co₂LAc⁺** and **Co₂L²⁺** was verified by electrospray ionization (ESI) and matrix-assisted laser desorption ionization (MALDI) mass spectrometry and Fourier transform infrared (FTIR) spectroscopy. FTIR spectra of **Co₂L²⁺** and **Co₂LAc⁺** show expected peaks for C=N stretches (ν = 1641−1629 cm⁻¹) (Figure S1 in the Supporting Information). Additionally, **Co₂LAc⁺** displays peaks for the bridging acetate ligand at ν_{as} = 1577 cm⁻¹ and ν_s = 1440 cm⁻¹. The lack of C=O stretches at 1680 cm⁻¹ confirms complete conversion of the aldehyde groups of 4-*tert*-butyl-2,6-diformylphenol into Schiff bases. Chemical oxidation of **Co₂L²⁺** with two equivalents of $NOPF_6$ in MeCN generates a diamagnetic sample as shown by ¹H NMR (Figure S2 in the Supporting Information), consistent with formation of low-spin $\mathbf{Co^{III}_2L^{4+}}$. The molar magnetic susceptibility (μ_{eff}) of **Co₂LAc⁺** in the solid state was measured at room temperature and found to be 5.32 μ_B. This value is lower than expected for ferromagnetically coupled high spin $(Co^{II})_2$ and is consistent with a weakly coupled antiferromagnetic spin state. Similar weak antiferromagnetic interactions between Co^{2+} ions have been observed for tetrakis-Schiff base macrocycles with N_6O_2 and N_4O_2 coordination environments.[37,38]

X-ray Crystal Structure. The crystal structure of **Co₂LAc⁺** is shown in Figure 1. Table 1 includes crystallographic data and structural refinement parameters. Unfortunately, all attempts to crystallize **Co₂L²⁺** were unsuccessful. **Co₂LAc⁺** crystallizes in the monoclinic space group $P2_1/n$ with nearly identical unit cell dimensions as Zn(II) and Mn(II) analogues (**Zn₂LAc⁺** and
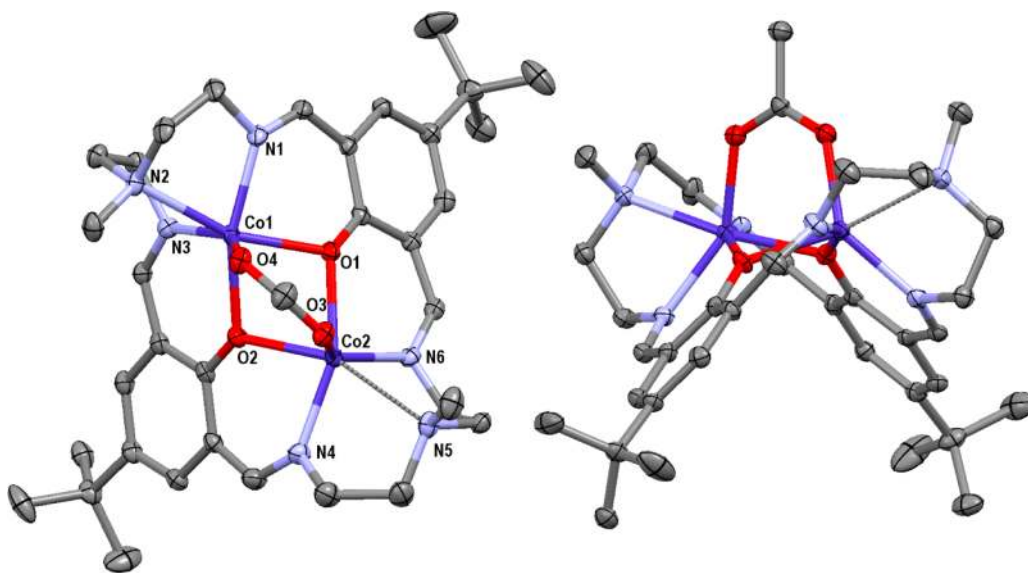

Figure 1. Top and side view ORTEP diagrams of $[\mathbf{Co_2LAc}](ClO_4)\cdot(CH_3CN)_{0.5}$ showing 50% probability thermal ellipsoids. Noncoordinating anion, hydrogen, and solvent atoms are omitted for clarity. The thin dashed lines represent elongated Co−N bonds (>2.50 Å).

Table 1. Crystallographic Data and Structural Refinement Parameters for [Co₂LAc](ClO₄)·(MeCN)₀.₅

	$[Co_2LAc](ClO_4) \cdot (MeCN)_{0.5}$
formula	$C_{74}H_{105}Co_4N_{13}O_{16}Cl_2$
fw	1739.33
cryst syst	monoclinic
space group	$P2_1/n$
a [Å]	12.290(3)
b [Å]	15.936(4)
c [Å]	21.465(5)
α [deg]	90
β [deg]	106.425(3)
γ [deg]	90
V [Å³]	4032.43(18)
Z	2
T [K]	100(2)
λ [Å]	0.710 73
ρ (calcd, g/cm³)	1.433
μ (mm⁻¹)	0.947
reflns collected	9431
no. of obs $[I > 2\sigma(I)]$	7804
refln/param ratio	18.86
R1[a] $[I > 2\sigma(I)]$	0.0488
wR2[b] $[I > 2\sigma(I)]$	0.1294
R1[a] (all data)	0.0591
wR2[b] (all data)	0.1388
GOF[c] on F^2	1.046

[a]$R1 = (\sum ||F_o| - |F_c||/\sum |F_o|)$. [b]$R_w(F_o^2) = [\sum [w(F_o^2 - F_c^2)^2]/\sum wF_o^4]^{1/2}$. [c]$GOF = [\sum [w(F_o^2 - F_c^2)^2]/(N_{obs} - N_{params})]^{1/2}$.

Mn₂LAc⁺) previously reported by us irrespective of counterions and crystallization solvent.[30] In addition, the structure of **Co₂LAc⁺** is very similar to the Zn(II) and Mn(II) analogues, save for the expected minor changes in bond lengths for the various metal ion sizes. Table 2 contains relevant bond distances and angles for **Co₂LAc⁺**. The N_6O_2 type macrocycle provides two pentadentate chelating environments for each of

Table 2. Selected Bond Distances (Å) and Angles (deg) for [Co₂LAc](ClO₄)·(MeCN)₀.₅ from the X-ray Crystallographic Analysis

		bond distances (Å)
	Co1−Co2	3.22
phenol	Co1−O1	2.0796(17)
phenol	Co1−O2	2.1422(17)
acetate	Co1−O4	2.0465(18)
imine	Co1−N1	2.074(2)
amine	Co1−N2	2.335(2)
imine	Co1−N3	2.089(2)
phenol	Co2−O1	2.1804(17)
phenol	Co2−O2	2.0772(17)
acetate	Co2−O3	2.0200(18)
imine	Co2−N4	2.067(2)
amine	Co2−N5	2.558
imine	Co2−N6	2.083(2)
		bond angles (deg)
	O2−Co1−O1	74.30(7)
	O1−Co2−O2	73.54(6)
	Co2−O1−Co1	98.19(7)
	Co1−O2−Co2	99.49(7)

the Co(II) centers holding them at 3.22 Å apart. Each of the Co(II) centers are in a highly distorted octahedral geometry with the bridging acetate group occupying the sixth coordination site. There is a slight asymmetry in the coordination environment around the two Co(II) centers, with one of the Co−N(amine) bonds elongated by 0.22 Å as compared to the other. The rest of the bonds in the primary coordination sphere are roughly symmetric. Most dinuclear tetrakis-Schiff base complexes with N_4O_2 type coordination environments result in a planar structure.[39−47] In contrast, increasing the chelating ability of the macrocycle by introducing N-methyl-2,2′-diaminodiethyldiamine into the ligand framework drastically distorts the geometry of complex, resulting in a twisted "butterfly-like" structure.[30−35,48]

Electronic Spectra. The ground state electronic absorption spectra of **Co₂L²⁺**, **Co₂LAc⁺**, **H₄L²⁺**, and **Zn₂LAc⁺** in MeCN are shown in Figure 2. The dinuclear tetrakis-Schiff base complexes
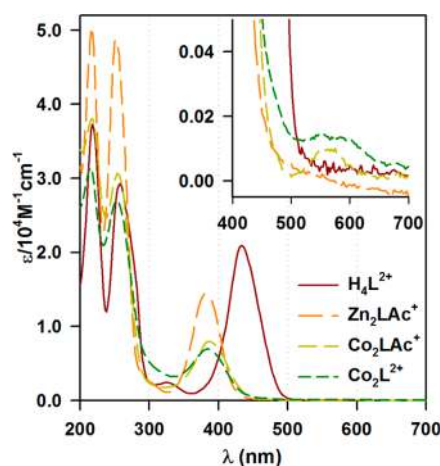
Figure 2. Comparison of UV−visible absorbance spectra of **Co₂L²⁺** (dark green), **Co₂LAc⁺** (green), **Zn₂LAc⁺** (orange), and **H₄L²⁺** (dark red) in MeCN. Inset: Enlarged view of the absorbance centered at 575 nm highlighting the Co(II) d−d transition for **Co₂L²⁺** and **Co₂LAc⁺**.

exhibit three primary absorbance bands in the UV−visible region at ∼215, 250, and 385 nm. Each of these bands is assigned to the π−π* transition from the tetrakis-Schiff base macrocycle ligand (i.e., phenolate and the ligand framework).[31,45,49,50] Because of the pronounced involvement of the π orbitals from the azomethine group in the lowest energy π−π* transition of the ligand framework, this band is sensitive to the charge on the metal ions.[30,51] A red shift to 434 nm is observed for **H₄L²⁺** due to the high charge density as compared to the metal dications.[30] A weak transition is also observed at 570 nm for **Co₂L²⁺** and **Co₂LAc⁺**, which may be attributed to a Co(II) d−d transition (Figure 2, inset).[52]

Electrochemistry. Figure 3 shows cyclic voltammograms (CV) of **Co₂L²⁺**, **Co₂LAc⁺**, **Zn₂LAc⁺**, and **H₄L²⁺** in anhydrous MeCN under N_2. All electrochemical potentials described herein are referenced to ferrocinium/ferrocene (Fc⁺/⁰) as an internal standard following the completion of each experiment.[53] Electrochemical analysis of **Zn₂LAc⁺** and **H₄L²⁺** enabled us to characterize the redox properties of the tetrakis-Schiff base ligand framework and thus helped distinguish the metal centered redox processes in **Co₂LAc⁺** and **Co₂L²⁺**. CVs of **Zn₂LAc⁺** and **H₄L²⁺** (Figure 3, traces c and d) showed two irreversible oxidation waves starting at approximately +0.88 V corresponding to individual phenolate
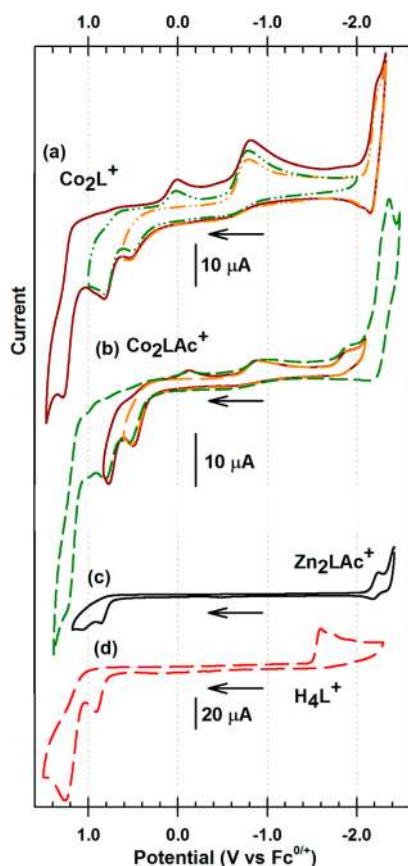
Figure 3. CVs of (a) Co_2L^{2+}, (b) Co_2LAc^+, (c) Zn_2LAc^+, and (d) H_4L^{2+}. All electrochemical scans were performed with 0.1 M $TBAPF_6$ supporting electrolyte in anhydrous MeCN at ν = 100 mV/s, with a glassy carbon working electrode, and platinum wire counter electrode. Arrows indicate initial scan direction; scans start at 0 V.

oxidations.[31,54−60] Reductive waves are also seen at −2.20 and −1.57 V for Zn_2LAc^+ and H_4L^{2+}, respectively, which are attributed to reduction of the imines.[61]

CVs of Co_2LAc^+ and Co_2L^{2+} also show ligand-centered reductions at −2.28 V and oxidations at +1.22 V, the latter of which occur at higher potentials as compared to Zn_2LAc^+ and H_4L^{2+} due to the higher positive charge of the two Co^{3+} centers as opposed to Zn^{2+} and H^+.[30] In addition to the ligand-based redox waves, there are numerous peaks in between resulting from Co-centered oxidations and reductions. Cathodic scans of Co_2L^{2+} reveal a reductive wave at +0.02 V, assigned as $Co^{III}_2/Co^{II}Co^{III}$, and a multielectron wave starting at about −0.68 V that includes the $Co^{II}Co^{III}/Co^{II}_2$ transition. The corresponding oxidation waves for each of the $Co^{II}_2/Co^{II}Co^{III}$ and $Co^{II}Co^{III}/Co^{III}_2$ redox couples are shifted significantly to higher potentials, resulting in relatively large peak splitting ($\Delta E_p = E_{pa} − E_{pc}$) of 0.72 and 0.42 V. Confirming their couple redox processes, the cathodic peak at +0.02 is not observed unless the preceding anodic scan extends past the second oxidation wave (Figure S3 in the Supporting Information). The non-Nernstian behavior of these transitions indicates a high degree of reorganization from changes in the Co spin state and likely distortions of coordination environment.[50,52] The CVs for Co_2LAc^{2+} are similar to Co_2L^{2+} with the $Co^{III}_2/Co^{II}Co^{III}$ reduction at −0.12 V and a multielectron wave at −0.83 V including the $Co^{II}Co^{III}/Co^{II}_2$ transition, but also display an additional cathodic wave at −1.88 V. Large ΔE_p for the $Co^{II}_2/$

$Co^{II}Co^{III}$ and $Co^{II}Co^{III}/Co^{III}_2$ oxidations are similar to Co_2L^{2+} at 0.82 and 0.51 V respectively. The scan rate dependence for each of the Co redox transitions for Co_2LAc^+ and Co_2L^{2+} shows a linear increase of peak current with higher $\nu^{1/2}$, indicating a diffusion controlled solution species (Figure S4 in the Supporting Information).[62]

Returning to the cathodic waves at approximately −0.78 V for Co_2L^{2+} and Co_2LAc^+ reveals a significantly higher charge as compared to other Co centered waves, suggesting a multielectron process. The charge associated with these multielectron waves shows a strong dependence on the starting potential and anodic end point of the previous scan, as shown in Figure S3 in the Supporting Information. When the CVs were reversed prior to oxidizing Co^{II}_2 to $Co^{II}Co^{III}$ (anodic waves at ∼+0.42 V), the charge passed (from −0.68 to −1.18 V) decreased by approximately one-third for Co_2L^{2+} and one-half for Co_2LAc^+. The multielectron nature of the cathodic wave from −0.78 to −1.18 V for Co_2L^{2+} can be seen in higher scan rate CVs in Figure 4. The CVs of Co_2L^{2+} obtained at
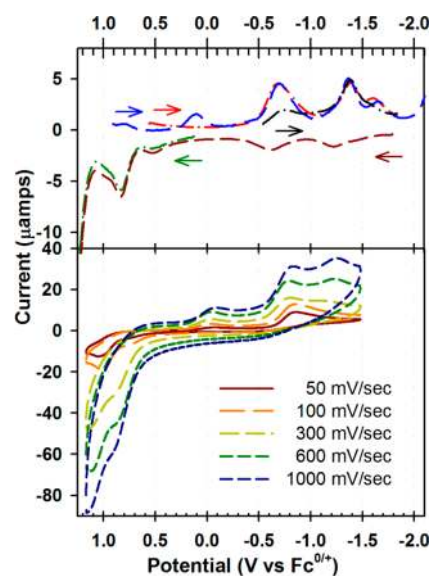

Figure 4. CVs of Co_2L^{2+} performed at 298 K with 0.1 M $TBAPF_6$ supporting electrolyte in anhydrous MeCN at various scan rates.

relatively slow scan rates of 50 and 100 mV/s show a single broad cathodic peak from −0.78 to −1.38 V, whereas faster scan rates clearly show two distinct waves at −0.78 and −1.33 V. Comparison of the charge passed for the cathodic processes at the faster scan rates (600 and 1000 mV/s) when normalized to $Co^{III}_2/Co^{II}Co^{III}$ reduction at +0.02 V is consistent with a $2e^−$ process at −0.78 V and $1e^−$ at −1.33 V. Cathodic differential pulse voltammetry (DPV) scans of Co_2L^{2+} also show multiple reduction waves in this potential range (Figure 4, top). In addition, when the DPV scan is initiated in the Co^{II}_2 redox state, the peak current at −0.78 V is reduced (Figure 4, top, black trace). Taken together, the combined cathodic peak from −0.78 to −1.38 V for Co_2L^{2+} is assigned as three closely spaced single electron reductions of $Co^{II}Co^{III}/Co^{II}_2$, $Co^{II}_2/Co^{II}Co^I$, and finally $Co^{II}Co^I/Co^I_2$. We surmise that, following the electrochemically slow $Co^{II}Co^{III}/Co^{II}_2$ reduction process in Co_2L^{2+}, the resulting coordination environment (including solvent binding) and spin states of the Co^{II} ions are more amenable to reduction to Co^I, resulting in the overlapping multielectron waves. The lack of a clear cathodic wave for the

$Co^{II}Co^I/Co^I_2$ redox process at slow scan rates could also be due to a competing chemical step following the formation of $Co^{II}Co^I$ that does not lead to Co^I_2. At higher scan rates, the $Co^{II}Co^I/Co^I_2$ redox process is kinetically competitive, resulting in the appearance of the cathodic wave at −1.33 V. In the CVs of **Co_2LAc^{2+}**, the charge passed for cathodic peak at −0.83 V only accounts for a 2e⁻ process when normalized to the Co^{III}_2/$Co^{II}Co^{III}$ reduction at −0.12 V, consistent with $Co^{II}Co^{III}/Co^{II}_2$ and $Co^{II}_2/Co^{II}Co^I$ reductions. The additional cathodic wave at −1.88 V for **Co_2LAc^{2+}** is assigned as the $Co^{II}Co^I/Co^I_2$ redox process. The presence of the coordinated acetate ion in **Co_2LAc^+** is sufficient to separate the $Co^{II}_2/Co^{II}Co^I$ and $Co^{II}Co^I/Co^I_2$ reductions, pushing the second reduction to −1.88 V.

Electrocatalytic H⁺ Reduction. To explore the possibility of **Co_2L^{2+}** to catalyze H⁺ reduction, we investigated its electrochemical response in anhydrous MeCN using a glassy carbon working electrode with increasing concentrations of TFA (pK_a = 12.7 in MeCN) and AcOH (pK_a = 22.3 in MeCN) as H⁺ sources.[63] The thermodynamic reduction potential of the acid $E°(AH/A^-;H_2)$ can be related its pK_a via eq 1,

$$E°(AH/A^-; H_2) = E°(H^+/H_2) - 2.3(RT/F)pK_{a(HA)}$$
(1)

Roberts and Bullock recently measured the standard reduction potential of H⁺ in acetonitrile, $E°(H^+/H_2)$, via open circuit potential measurements and determined it to be −0.028 ± 0.008 V vs Fc⁺/⁰.[64] At standard conditions, $E°(AH/A^-;H_2)$ would be −0.78 and −1.35 V vs Fc⁺/⁰ for TFA and AcOH respectively, but at high concentrations of the acid alone (unbuffered), homoconjugation leads to an increase in effective acidity and a lowering of the standard reduction potential.[64−66] CVs of **Co_2L^{2+}** in the presence of increasing amounts of TFA show an irreversible catalytic reduction wave starting at about −1.28 V (Figure 5a), which is close to the potential for the $Co^{II}Co^I/Co^I_2$ redox couple of **Co_2L^{2+}** (see discussion above). This effect is more discernible in DPV scans of **Co_2L^{2+}** in the presence of increasing TFA (Figure S5 in the Supporting Information), where the reduction wave initiates at the same potential as the $Co^{II}Co^I/Co^I_2$ redox couple. The magnitude of this catalytic wave in Figure 5a is significantly higher than the Faradaic responses of the $Co^{II}Co^{III}/Co^{II}_2$ redox processes at −0.78 V, which remain largely unchanged at different TFA concentrations. The current evolved during this irreversible cathodic wave is directly proportional to concentration of TFA in the electrolyte, which is consistent with electrocatalytic H⁺ reduction.[19,61,67−70] The waves also exhibit a plateau at about −1.88 V, indicating that the catalytic reaction is sufficiently rapid that the current is partially controlled by diffusion of H⁺ to the electrode surface.[20,71,72] The potential at $i_{cat/2}$ ($E_{cat/2}$) at 5 mM and 55 mM TFA was −1.58 V and −1.66 V respectively.

The catalytic peak current (i_c) at −1.88 V for H⁺ reduction was observed to vary linearly with [TFA], suggesting a second order rate dependence. Furthermore, i_c also varied linearly with [**Co_2L^{2+}**], indicating a first order dependence in catalyst (Figure 6). This is consistent with electrocatalytic H⁺ reduction, suggesting that under these conditions the catalytic peak current (i_c) is related to the concentration of the catalyst and acid by eq 2,[62,67]
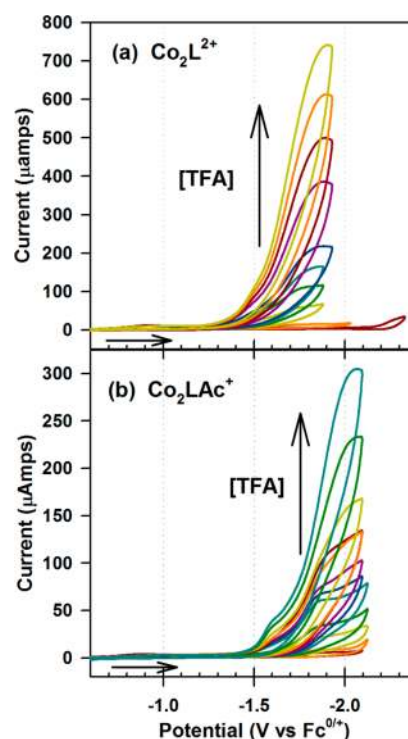
$$i_c = n_cFAC\sqrt{Dk[H^+]^2}$$
(2)

Figure 5. CVs of 1 mM **Co_2L^{2+}** (a) and **Co_2LAc^+** (b) in 0.1 M TBAPF₆/MeCN upon addition of increasing amounts of TFA (1−65 mM) as indicated by the vertical arrow in the figure. CVs were performed at 298 K, with a scan rate of ν = 100 mV/s. The horizontal arrow indicates initial direction of scan. The CVs were stopped prior to −2.18 V to avoid complications from ligand reduction.
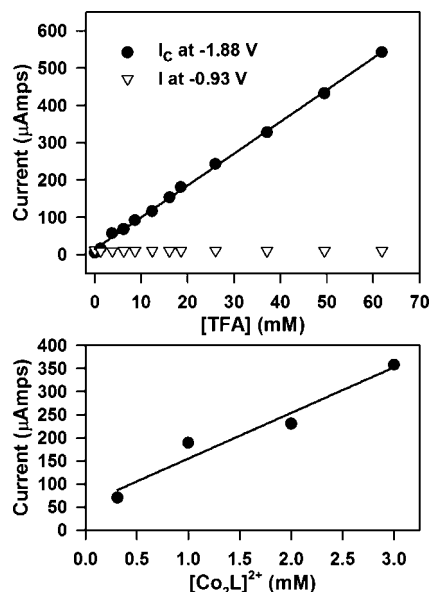
Figure 6. Top: Background corrected electrocatalytic current (i_c, filled circles) at −1.88 V for 1 mM of **Co_2L^{2+}** as a function of [TFA]. The Faradaic current for the $Co^{II}Co^{III}/Co^{II}_2$ redox transition at −0.93 V is shown as open triangles. Bottom: Electrocatalytic current in the presence of 25 mM TFA as a function of varying [**Co_2L^{2+}**]. Cyclic voltammetry was done at 298 K, ν = 100 mV/s, and 0.1 M TBAPF₆ solution in anhydrous MeCN under N₂.

where n_c = 2, the number of electrons involved in the catalytic process, F is the Faraday constant, A is the electrode surface

area, C is the catalyst concentration, k is the catalytic rate constant, and D is the diffusion coefficient of Co_2L^{2+}. For a noncatalytic redox wave in CV scans obeying Nernstian behavior, the Faradaic peak current (i_p) follows the Randles−Sevick equation[62]

$$i_p = 0.4463 n_p FAC \sqrt{nF\nu D/RT} \qquad (3)$$

where n_p = number of electrons involved in the redox process, ν is scan rate, R is the universal gas constant, and T is temperature (K). Comparing the ratio of catalytic (i_c) to noncatalytic (i_p) currents via eq 4 allows for the straightforward determination of the electrocatalytic rate without prior determination of D.

$$\frac{i_c}{i_p} = 2.242 \frac{n_c}{n_p} \sqrt{\frac{kRT[H^+]^2}{n_p F \nu}} \qquad (4)$$

Due to the absence of an ideal one electron redox process for Co_2L^{2+} we have used the $Co_2^{III,III}/Co^{II}Co^{III}$ reduction at 0.08 V as a one electron noncatalytic peak (i_p) to obtain an approximate k from eq 4.[73,74] Since this is an electrochemically nonreversible oxidation, the value of i_p is likely smaller than that of a reversible oxidation. Consequently, the rate obtained from this analysis may be higher than the actual rate. This analysis was developed for catalytic systems following a simple EC mechanism; however, numerous groups have applied this methodology to more complicated catalytic systems, allowing them to compare catalytic rates for a range of complexes.[20,67,69,75] The catalytic rate constant (k) obtained for Co_2L^{2+} by comparing the ratio of i_c/i_p over a range of scan rates (ν) (Figure S6 in the Supporting Information) is ∼138 M^{-2} s^{-1}.

A similar electrocatalytic study was performed with Co_2LAc^+ to investigate the effect of acetate coordination and potential inhibition of H^+ reduction. As shown in Figure 5b, CVs of 1 mM solution of Co_2LAc^+ in the presence of excess TFA showed an electrocatalytic wave close to that of the $Co^{II}Co^I/Co^I_2$ redox couple, similar to Co_2L^{2+}. The electrocatalytic waves are shifted to more reducing potentials than that of Co_2L^{2+} and are preceded by a shoulder at −1.58 V. The shift in catalytic current to more reducing potentials, as compared to Co_2L^{2+}, is likely due to activation of the complex for H^+ reduction via acetate dissociation at the potential for $Co_2^{II,I}/Co^I_2$ reduction. Similar to Co_2L^{2+}, the catalytic peak current (i_c) at −2.0 V was found to have a second order rate dependence on [TFA] and first order in [Co_2LAc^+] (Figure S7 in the Supporting Information). The catalytic rate (k) obtained from eq 3 for Co_2LAc^+ (Figure S8 in the Supporting Information) is ∼63 M^{-2} s^{-1}. This rate is slightly lower than that of Co_2L^{2+}, suggesting that acetate dissociation may be a limiting factor on the electrochemical time scale.

The electrocatalytic response of Co_2L^{2+} was also compared to background signals from the glassy carbon electrode under similar conditions. CVs of Co_2L^{2+} show a significantly higher current and lower onset potential for the electrocatalytic wave as compared to CVs of the bare electrode at three different concentrations of TFA (Figure S9 in the Supporting Information). Additionally, to eliminate the possibility of a pseudocatalytic current arising from heterogeneous Co species deposited on electrode during the electrocatalytic scans, we removed the electrode after scanning Co_2L^{2+} in the presence of 5 equiv of TFA and placed the same uncleaned electrode in fresh electrolyte (without Co_2L^{2+}) with and without 5 equiv of

TFA. The repeated CV scans of the uncleaned electrode show similar currents to background, suggesting that the initial electrocatalytic waves for Co_2L^{2+} are due to homogeneous H^+ reduction (Figure S9 in the Supporting Information).

The electrocatalytic activity of Co_2L^{2+} was also investigated using AcOH as the H^+ source (Figure 7). CVs of Co_2L^{2+} with
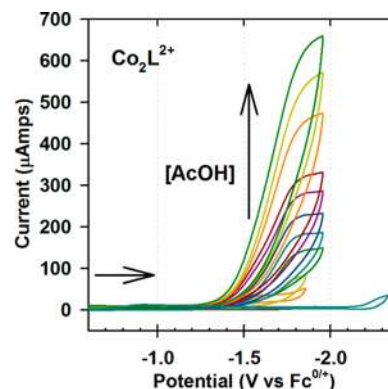

Figure 7. CVs of 1 mM Co_2L^{2+} in 0.1 M $TBAPF_6$/MeCN upon addition of increasing amounts of AcOH (1−65 mM) as indicated by the vertical arrow in the figure. CVs were performed at 298 K, with a scan rate of ν = 100 mV/s. The horizontal arrow indicates initial direction of scan.

increasing concentration of AcOH displayed similar electro-catalytic waves to those with TFA, initiating at −1.28 V and reaching a peak at −1.88 V. $E_{cat/2}$ for Co_2L^{2+} with 5 mM and 55 mM AcOH was −1.68 V and −1.66 V respectively. The catalytic current at −1.88 V showed linear first order dependence on [AcOH] (Figure S10 in the Supporting Information) and a second order dependence on [Co_2L^{2+}] at constant acid concentrations (Figure S11 in the Supporting Information, left) and constant acid equivalence (Figure S11 in the Supporting Information, right). AcOH being a weaker acid than TFA, the onset potential for reduction of AcOH at the bare electrode is expected to be at a lower potential than TFA. This is manifested when we perform electrocatalysis at an uncleaned electrode (removed after scanning Co_2L^{2+} in the presence of 5 equiv of AcOH). With the unclean electrode placed in fresh electrolyte without Co_2L^{2+}, with and without 5 equiv of AcOH, we observed very negligible current at −1.38 to −1.88 V (Figure S12 in the Supporting Information). In addition, the catalytic current (i_c) reaches a limiting current at high H^+ concentration (>400 mM TFA and >1000 mM AcOH) (Figure S13 in the Supporting Information). These results with both TFA and AcOH as the proton source support our hypothesis of homogeneous H^+ reduction using Co_2L^{2+}.

In order to characterize the product of electrocatalysis, controlled potential electrolysis (CPE) of 1 mM Co_2L^{2+} was carried out at −1.88 V in the presence of 100 mM AcOH in MeCN, with stirring in a sealed flask sparged with N_2 (Figure S14 in the Supporting Information). A piece of carbon paper was used as the working electrode and gave a nearly identical CV for Co_2L^{2+} as those shown in Figure 3 and Figure 5. The head space above the electrolyte solution was examined by gas chromatography (GC) at various time points throughout the CPE, and H_2 was detected in 72−94% Faradaic efficiency (Figure S14 in the Supporting Information).

Interestingly, the onset potential and peak potential for the H^+ electrocatalytic reduction wave for Co_2L^{2+} were the same

irrespective of these acids, which suggests a similar mechanism. The electrocatalytic wave initiates at the tail of the multi-electron wave where Co^I_2 is formed (see discussion above), ~ -1.28 V. This suggests that the formation of $[Co^I_2L]^0$, or its redox equivalent, is required to initiate H_2 production. The 3.22 Å Co−Co distance seen in the crystal structure of Co_2LAc^+ is likely too long to involve a bridging hydride as most known $Co_2(\mu\text{-H})$ have Co−Co distance in the range of 2.2−2.3 Å.[76,77] One potential pathway consistent with the electrocatalytic wave initiating at −0.9 V would involve the sequential two electron reductions and protonations of $[Co^{II}Co^{II}]$ to generate $[Co^{III}HCo^{III}H]$, which could then undergo intramolecular homolysis to give $[Co^{II}Co^{II}]$ and H_2. This pathway differs from that of the dicobalt complex of Llobet, Fukuzumi, and co-workers which only requires reduction to the $[Co^{II}Co^I]$ state and protonation to give $[Co^{II}Co^{III}−H]$, which subsequently undergoes heterolytic attack by a second H^+ to generate H_2.[28] Alternatively, reduction of Co_2L^{2+} to $[Co^{II}Co^I]$ could generate $[Co^{II}Co^{III}H]$ in the presence of H^+. Subsequent reduction to $[Co^{II}Co^{II}H]$ may be favored over $[Co^ICo^{III}H]$, which could then be followed by heterolytic attack by a second H^+ to generate H_2. Both of these pathways would be consistent with electrocatalytic wave starting at −1.28 V that is first order in [catalyst] and second order in [acid], but further examination will be required to clarify the exact process.

The electrochemical response of Zn_2LAc^+ in the presence of TFA was also investigated as a control study, as the central redox inactive Zn^{II} ions are not expected to participate in H^+ reduction. In the absence of acid, Zn_2LAc^+ displayed a reduction wave at −2.18 V. Upon addition of TFA, a large irreversible reduction begins to appear at −1.53 V, similar to what is observed for H_4L^{2+}. The peak current for this cathodic wave reaches a plateau at 17 mM TFA and is consistent with demetalation of Zn_2LAc^+ leading to in situ formation of H_4L^{2+} (Figure S15 in the Supporting Information). This is further supported by UV−visible absorbance changes of Zn_2LAc^+ in the presence of TFA (vide infra). Each of the tetrakis-Schiff base macrocyles have four imine (C=N) bonds that are susceptible to reductive hydrogenation in the presence of acid, which may result in the appearance of a pseudocatalytic wave as reported by Saveant for a tris(glyoximato) cobalt complex.[61] While the irreversible reduction waves for Zn_2LAc^+ reached an asymptotic upper limit (Figure S15 in the Supporting Information), the electrocatalytic waves for Co_2L^{2+} and Co_2LAc^+ continue to increase with TFA concentration higher than H^+ equivalents required for imine reduction (Figure 6). Finally, to investigate the stability of the Schiff base complexes in the presence of excess acid, we monitored the change in absorbance for Co_2L^{2+}, Co_2LAc^+, and Zn_2LAc^+ in anhydrous MeCN with subsequent additions of 65 equiv of TFA (Figure S16 in the Supporting Information). We observed insignificant changes in absorbance for Co_2L^{2+} and Co_2LAc^+ after several hours, suggesting that the compounds stay intact in the presence of excess TFA. Zn_2LAc^+, on the other hand, showed a rapid red shift of the peak at 385 to 430 nm, suggesting that Zn_2LAc^+ undergoes demetalation. The stability of Co_2L^{2+} and Co_2LAc^+ in the presence of 65 equiv of TFA was validated by MALDI MS (Figure S16 in the Supporting Information), showing M^+ ion peaks at m/z 803.98 for both the complexes, which indicates CF_3COO^- adduct formation. We observe a less intense peak at m/z 632.1, corresponding to the loss of one Co from Co_2L^{2+} and Co_2LAc^+. In contrast, for Zn_2LAc^+ we observed M^+ peaks only at m/z 637.05 and 575.10

corresponding to loss of one and two zinc atoms respectively from Zn_2LAc^+, as expected. It is worth noting that no parent ion peak at m/z 759.2 corresponding to Zn_2LAc^+ was observed. This is consistent with our hypothesis of demetalation of Zn from electrocatalysis of Zn_2LAc^+ in the presence of TFA, whereas Co_2L^{2+} and Co_2LAc^+ remain stable over the course of several hours.

CONCLUSION

The results from this study show that a new class of dicobalt tetrakis-Schiff base complexes, Co_2L^{2+} and Co_2LAc^+, are capable of electrocatalytic H^+ reduction in anhydrous MeCN using both TFA and AcOH as proton sources. CPE electrolysis of Co_2L^{2+} with AcOH generated H_2 in 72−94% Faradaic efficiency. Despite the relatively high overpotential required to drive catalysis, this class of complexes gives us a chance to explore different dinuclear sites for catalytic H^+ reduction. Electrocatalytic H^+ reduction initiates at potential required to reduce the bimetallic site from $Co_2^{II,II}$ to Co^I_2. Based on the prevailing reaction pathways reported in the literature for other cobalt-based electrocatalysts, we postulate that catalytic H^+ reduction in Co_2L^{2+} and Co_2LAc^+ is initiated by the formation of $[Co^{III}−H]$ intermediates from Co^I and H^+.[4,20,67,78] Due to the close proximity of the two Co ions in Co_2L^{2+} and Co_2LAc^+ (3.2 Å), the catalytic mechanism may also involve bimetallic intermediates in the form of adjacent $[Co^{III}−H]_2$, or heterolytic attack of H^+ on $[Co^{II}Co^{II}H]$. Furthermore, the strong chelating nature of the N_6O_2 ligand may assist in the stability of the complex at low pH and low metal oxidation states. We are currently working toward full identification of the intermediate states and determination of a mechanistic cycle, as well as developing synthetic modifications to the ligand framework to shift the $Co_2^{II,I}/Co^I_2$ reduction to more positive potentials.

EXPERIMENTAL SECTION

General Methods. MALDI-TOF MS were obtained on a Bruker Ultraflex III. LR and HR ESI MS were obtained on a Thermo Electron Finnigan TSQ Quantum Ultra. Elemental analyses were obtained from Atlantic Microlabs, Inc., Norcross, GA. Electronic absorption spectra were obtained using a PerkinElmer Lambda 950 or Agilent 8453A spectrophotometer with a 1.0 cm quartz cell under a nitrogen atmosphere. Infrared absorption spectra were acquired using a Biorad Excalibur FTS-3000MX equipped with a liquid N_2-cooled MCT detector.

Materials. 4-*tert*-Butyl-2,6-diformylphenol was purchased from Sigma-Aldrich and was purified by column chromatography on silica gel with methylene chloride. All other chemicals and solvents used were of the highest purity available from commercial suppliers. MeCN was dried by circulating the N_2-purged solvent through a solid-state column purification system (Vacuum Atmospheres Company, Hawthorne, CA) prior to use.[79] Tetrabutylammonium hexafluor-ophosphate ($TBAPF_6$) was purchased from Acros and twice recrystallized from hot ethanol before use in electrochemical experiments. $[Zn_2LAc](ClO_4)$ and $[H_4L](ClO_4)_2$ were available from a previous study.[30] *Caution! Perchlorate salts of metal complexes with organic ligands are potentially explosive. Only small quantities of these compounds should be prepared and handled behind suitable protective shield.*

[Co_2L](ClO_4)_2. $Co(ClO_4)_2\cdot6H_2O$ (200 mg, 0.55 mmol) and 4-*tert*-butyl-2,6-diformylphenol (100 mg, 0.48 mmol) were dissolved in 10 mL of methanol and purged with N_2. To this solution was added N′-methyl-2,2′-diaminodiethyldiamine (62 μL, 0.48 mmol) dissolved in 1 mL of methanol dropwise while stirring. The mixture was refluxed for 4 h under N_2, then cooled, and the volume of the solvent reduced under vacuum to approximately 2−3 mL. The resulting solution was kept at 0 °C for 24 h, yielding a brown powder, which was filtered and

washed with cold methanol, followed by anhydrous diethyl ether. Successive recrystallizations from dichloromethane with diethyl ether gave $[\mathbf{Co_2L}](ClO_4)_2$ (mass 189 mg, 78% yield). MALDI LR-MS (m/z): 789.18 $[M - (ClO_4)]^+$. ESI LR-MS (m/z): 735.25 $[M - 2(ClO_4) + (HCOO)]^+$, 344.62 $[M - 2(ClO_4)]^{2+}$. ESI HR-MS: Calcd for $[M - 2(ClO_4) + (HCOO)]^+$ 735.2474, found 735.2487. Anal. Calcd for $C_{34}H_{48}N_6O_{10}Co_2Cl_2(H_2O)_3$: C, 43.27; H, 5.76; N, 8.90. Found: C, 43.73; H, 5.51; N, 8.29.

$[Co_2LAc](ClO_4)$. $Co(ClO_4)_2 \cdot 6H_2O$ (200 mg, 0.55 mmol), 4-*tert*-butyl-2,6-diformylphenol (100 mg, 0.48 mmol), and sodium acetate (97 mg, 1.18 mmol) were dissolved in 10 mL of methanol and purged with nitrogen. To this solution was added N'-methyl-2,2′-diamino-diethyldiamine (62 μL, 0.48 mmol) dissolved in 1 mL of methanol dropwise while stirring. The mixture was refluxed for 4 h under nitrogen, then cooled, and the volume of the solvent reduced under reduced pressure to 2−3 mL. The resulting solution was kept at 0 °C for 24 h, which yielded dark brown-maroon powder product. This was filtered and washed with cold methanol followed by anhydrous diethyl ether. Successive recrystallizations from dichloromethane with diethyl ether gave $[\mathbf{Co_2LAc}](ClO_4)$ (mass 181 mg, 70% yield). MALDI LR-MS (m/z): 749.26 $[M − ClO_4]^+$. ESI LR-MS (m/z): 749.26 $[M − ClO_4]^+$. ESI HR-MS: Calcd for $[M − (ClO_4)]^+$ 749.2630, found 749.2615. Calcd for $[M − (ClO_4) − (CH_3COO)]^{2+}$ 345.1246, found 345.1250. Anal. Calcd for $C_{36}H_{51}N_6O_8Co_2Cl(H_2O)_4$: C, 46.93; H, 6.45; N, 9.12. Found: C, 46.09; H, 5.86; N, 9.44.

Magnetic Susceptibility. The magnetic susceptibility of $[\mathbf{Co_2LAc}](ClO_4)$ was measured on a Johnson Matthey (Mark1) magnetic susceptibility meter at room temperature (298 K) and corrected for diamagnetic contributions using Pascal's constants.

Crystal Structure Determinations and Refinement. Crystals of $[\mathbf{Co_2LAc}](ClO_4)$ suitable for X-ray crystallography were obtained by slow diffusion of diethyl ether into a saturated solution of $[\mathbf{Co_2LAc}](ClO_4)$ in MeCN. Data collection was performed on a Bruker SMART APEX CCD-based X-ray diffractometer with graphite-monochromated Mo Kα radiation ($\lambda = 0.71073$ Å) at $T = 100(2)$ K. The frames were integrated with the Bruker SAINT software package,[80] and data were corrected for absorption effects using the empirical method SADABS.[81] The structure was solved by direct methods and refined using the Bruker SHELXTL software package.[82,83] Hydrogen atoms were included at idealized positions using the riding model.

Electrochemistry. Electrochemical experiments were performed using a CHI440A (CH Instruments, Austin, TX) potentiostat and analyzed using CHI version 7.31 software. Electrolyte solutions (0.1 M tetrabutylammonium hexafluorophosphate, $TBAPF_6$) were prepared with anhydrous solvents (from SPS) and deoxygenated with nitrogen prior to use. All electrochemical experiments were performed under N_2 and anhydrous solvents with potentials reported versus SCE via $Fc^{0/+}$ as an internal standard and a silver wire pseudoreference electrode.[53,62] A Pt wire was used as the counter electrode, and a glassy carbon macro disk electrode (diameter = 0.29 cm) was used as the working electrode. DPV scans had a 4 mV step potential, 50 mV amplitude, 100 ms pulse width, and pulse period of 300 ms.

Controlled Potential Electrolysis and Headspace Analysis. Controlled potential electrolysis (CPE) was carried out in a 150 mL 2-neck round-bottom flask, using a Ag wire reference electrode, Pt foil counter electrode, and a 4 cm × 2 cm carbon paper (Fuel Cell Earth, part # MGL280) as the working electrode. Electrolyte solutions were 0.1 M $TBAPF_6$ in anhydrous acetonitrile. The flask and electrolyte were purged with N_2 for ca. 30 min before conducting the CPE. The headspace was sampled with a gastight syringe and analyzed with a Gow-Mac series 350 gas chromatograph equiped with a molecular sieve 13X column, a thermal conductivity detector, and argon as the carrier gas. H_2 was also detected using a two compartment electrochemical cell with the working electrode separated from the counter by a glass frit.

■ ASSOCIATED CONTENT

ⓢ Supporting Information

Scheme depicting synthesis of $[\mathbf{Co_2L}](ClO_4)_2$ and $[\mathbf{Co_2LAc}]$-(ClO_4). Figures depicting FTIR and ^1H NMR spectra and electrochemical results. Crystallographic information in CIF format. This material is available free of charge via the Internet at http://pubs.acs.org.

■ AUTHOR INFORMATION

Corresponding Author

*E-mail: dinolp@rpi.edu.

Notes

The authors declare no competing financial interest.

■ ACKNOWLEDGMENTS

■ REFERENCES

(1) Artero, V.; Fontecave, M. *Coord. Chem. Rev.* **2005**, *249*, 1518−1535.

(2) Bakac, A.; Espenson, J. H. *J. Am. Chem. Soc.* **1984**, *106*, 5197−5202.

(3) Chao, T.-H.; Espenson, J. H. *J. Am. Chem. Soc.* **1978**, *100*, 129−133.

(4) Dempsey, J. L.; Brunschwig, B. S.; Winkler, J. R.; Gray, H. B. *Acc. Chem. Res.* **2009**, *42*, 1995−2004.

(5) McNamara, W. R.; Han, Z.; Alperin, P. J.; Brennessel, W. W.; Holland, P. L.; Eisenberg, R. *J. Am. Chem. Soc.* **2011**, *133*, 15368−15371.

(6) Krawicz, A.; Yang, J.; Anzenberg, E.; Yano, J.; Sharp, I. D.; Moore, G. F. *J. Am. Chem. Soc.* **2013**, *135*, 11861−11868.

(7) McCormick, T. M.; Calitree, B. D.; Orchard, A.; Kraut, N. D.; Bright, F. V.; Detty, M. R.; Eisenberg, R. *J. Am. Chem. Soc.* **2010**, *132*, 15480−15483.

(8) Dempsey, J. L.; Winkler, J. R.; Gray, H. B. *J. Am. Chem. Soc.* **2010**, *132*, 1060−1065.

(9) Du, P.; Schneider, J.; Luo, G.; Brennessel, W. W.; Eisenberg, R. *Inorg. Chem.* **2009**, *48*, 4952−4962.

(10) Razavet, M.; Artero, V.; Fontecave, M. *Inorg. Chem.* **2005**, *44*, 4786−4795.

(11) Baffert, C.; Artero, V.; Fontecave, M. *Inorg. Chem.* **2007**, *46*, 1817−1824.

(12) Fihri, A.; Artero, V.; Razavet, M.; Baffert, C.; Leibl, W.; Fontecave, M. *Angew. Chem., Int. Ed.* **2008**, *47*, 564−567.

(13) Fihri, A.; Artero, V.; Pereira, A.; Fontecave, M. *Dalton Trans.* **2008**, 5567−5569.

(14) Muckerman, J. T.; Fujita, E. *Chem. Commun.* **2011**, *47*, 12456−12458.

(15) Bhattacharjee, A.; Andreiadis, E. S.; Chavarot-Kerlidou, M.; Fontecave, M.; Field, M. J.; Artero, V. *Chem.—Eur. J.* **2013**, *19*, 15166−15174.

(16) Solis, B. H.; Hammes-Schiffer, S. *Inorg. Chem.* **2011**, *50*, 11252−11262.

(17) Du, P.; Knowles, K.; Eisenberg, R. *J. Am. Chem. Soc.* **2008**, *130*, 12576−12577.

(18) Lazarides, T.; McCormick, T.; Du, P.; Luo, G.; Lindley, B.; Eisenberg, R. *J. Am. Chem. Soc.* **2009**, *131*, 9192−9194.

(19) Hu, X.; Cossairt, B. M.; Brunschwig, B. S.; Lewis, N. S.; Peters, J. C. *Chem. Commun.* **2005**, 4723−4725.

(20) Hu, X.; Brunschwig, B. S.; Peters, J. C. *J. Am. Chem. Soc.* **2007**, *129*, 8988−8998.

(21) Probst, B.; Rodenberg, A.; Guttentag, M.; Hamm, P.; Alberto, R. *Inorg. Chem.* **2010**, *49*, 6453−6460.

(22) Chen, L.; Wang, M.; Gloaguen, F.; Zheng, D.; Zhang, P.; Sun, L. *Inorg. Chem.* **2013**, *52*, 1798−1806.

(23) da Graca Moraes Braga Martin, M.; Vidotti, M.; Nunes, F. S. *Int. J. Hydrogen Energy* **2012**, *37*, 14094−14102.

(24) Capon, J.-F.; Gloaguen, F.; Petillon, F. Y.; Schollhammer, P.; Talarmin, J. *Coord. Chem. Rev.* **2009**, *253*, 1476−1494.

(25) Surawatanawong, P.; Tye, J. W.; Darensbourg, M. Y.; Hall, M. B. *Dalton Trans.* **2010**, *39*, 3093−3104.

(26) Valdez, C. N.; Dempsey, J. L.; Brunschwig, B. S.; Winkler, J. R.; Gray, H. B. *Proc. Natl. Acad. Sci. U.S.A.* **2012**, *109*, 15589−15593.

(27) Szymczak, N. K.; Berben, L. A.; Peters, J. C. *Chem. Commun.* **2009**, 6729−6731.

(28) Mandal, S.; Shikano, S.; Yamada, Y.; Lee, Y.-M.; Nam, W.; Llobet, A.; Fukuzumi, S. *J. Am. Chem. Soc.* **2013**, *135*, 15294−15297.

(29) Pilkington, N. H.; Robson, R. *Aust. J. Chem.* **1970**, *23*, 2225−36.

(30) Kal, S.; Filatov, A. S.; Dinolfo, P. H. *Inorg. Chem.* **2013**, *52*, 13963−13973.

(31) Soler, M.; McCusker, J. K. *J. Am. Chem. Soc.* **2008**, *130*, 4708−4724.

(32) Nagata, T.; Ikawa, Y.; Maruyama, K. *J. Chem. Soc., Chem. Commun.* **1994**, 471−472.

(33) Qian, M.; Gou, S.; Yu, Z.; Ju, H.; Xu, Y.; Duan, C.; You, X. *Inorg. Chim. Acta* **2001**, *317*, 157−162.

(34) Nagata, T.; Mizukami, J. *J. Chem. Soc., Dalton Trans.* **1995**, 2825−2830.

(35) Ikawa, Y.; Nagata, T.; Maruyama, K. *Chem. Lett.* **1993**, *22*, 1049−1052.

(36) Dutta, B.; Bag, P.; Adhikary, B.; Flörke, U.; Nag, K. *J. Org. Chem.* **2004**, *69*, 5419−5427.

(37) Lambert, S. L.; Hendrickson, D. N. *Inorg. Chem.* **1979**, *18*, 2683−2686.

(38) Timken, M. D.; Marritt, W. A.; Hendrickson, D. N.; Gagne, R. A.; Sinn, E. *Inorg. Chem.* **1985**, *24*, 4202−4208.

(39) Hoskins, B. F.; Williams, G. A. *Aust. J. Chem.* **1975**, *28*, 2607−2614.

(40) Hoskins, B. F.; Robson, R.; Williams, G. A. *Inorg. Chim. Acta* **1976**, *16*, 121−133.

(41) Samulewski, R. B.; Cesar, d. R. J.; Fuganti, O.; Stieler, R.; Lang, E. S.; Fialho, V. M. d. G.; Nunes, F. S. *J. Mol. Struct.* **2010**, *984*, 354−358.

(42) Mandal, S. K.; Thompson, L. K.; Newlands, M. J.; Gabe, E. J. *Inorg. Chem.* **1989**, *28*, 3707−3713.

(43) Diril, H.; Chang, H.-R.; Zhang, X.; Larsen, S. K.; Potenza, J. A.; Pierpont, C. G.; Schugar, H. J.; Isied, S. S.; Hendrickson, D. N. *J. Am. Chem. Soc.* **1987**, *109*, 6207−6208.

(44) Chang, H.-R.; Larsen, S. K.; Boyd, P. D. W.; Pierpont, C. G.; Hendrickson, D. N. *J. Am. Chem. Soc.* **1988**, *110*, 4565−4576.

(45) Downard, A. J.; McKee, V.; Tandon, S. S. *Inorg. Chim. Acta* **1990**, *173*, 181−190.

(46) Wada, H.; Motoda, K.-i.; Ohba, M.; Sakiyama, H.; Matsumoto, N.; Okawa, H. *Bull. Chem. Soc. Jpn.* **1995**, *68*, 1105−1114.

(47) Liu, J.; Pan, Z.-Q.; Zhou, H.; Li, Y.-Z. *Acta Crystallogr., Sect. E: Struct. Rep. Online* **2008**, *64*, m1506−m15.

(48) Qian, M.; Gou, S.; Chantrapromma, S.; Sundara, R. S. S.; Fun, H. K.; Zeng, Q.; Yu, Z.; You, X. *Inorg. Chim. Acta* **2000**, *305*, 83−90.

(49) Cook, C. D.; Woodworth, R. C. *J. Am. Chem. Soc.* **1953**, *75*, 6242−6244.

(50) Böttcher, A.; Takeuchi, T.; Hardcastle, K. I.; Meade, T. J.; Gray, H. B.; Cwikel, D.; Kapon, M.; Dori, Z. *Inorg. Chem.* **1997**, *36*, 2498−2504.

(51) Bosnich, B. *J. Am. Chem. Soc.* **1968**, *90*, 627−632.

(52) Meghdadi, S.; Amirnasr, M.; Habibi, M. H.; Amiri, A.; Ghodsi, V.; Rohani, A.; Harrington, R. W.; Clegg, W. *Polyhedron* **2008**, *27*, 2771−2778.

(53) Pavlishchuk, V. V.; Addison, A. W. *Inorg. Chim. Acta* **2000**, *298*, 97−102.

(54) Kurahashi, T.; Kikuchi, A.; Tosha, T.; Shiro, Y.; Kitagawa, T.; Fujii, H. *Inorg. Chem.* **2008**, *47*, 1674−1686.

(55) Kurahashi, T.; Fujii, H. *J. Am. Chem. Soc.* **2011**, *133*, 8307−8316.

(56) Müller, J.; Kikuchi, A.; Bill, E.; Weyhermüller, T.; Hildebrandt, P.; Ould-Moussa, L.; Wieghardt, K. *Inorg. Chim. Acta* **2000**, *297*, 265−277.

(57) Goldberg, D. P.; Koulougliotis, D.; Brudvig, G. W.; Lippard, S. J. *J. Am. Chem. Soc.* **1995**, *117*, 3134−3144.

(58) Chaudhuri, P.; Wieghardt, K. *Prog. Inorg. Chem.* **2002**, 151−216.

(59) Bill, E.; Müller, J.; Weyhermüller, T.; Wieghardt, K. *Inorg. Chem.* **1999**, *38*, 5795−5802.

(60) Sokolowski, A.; Müller, J.; Weyhermüller, T.; Schnepf, R.; Hildebrandt, P.; Hildenbrand, K.; Bothe, E.; Wieghardt, K. *J. Am. Chem. Soc.* **1997**, *119*, 8889−8900.

(61) Anxolabéhère-Mallart, E.; Costentin, C.; Fournier, M.; Nowak, S.; Robert, M.; Savéant, J.-M. *J. Am. Chem. Soc.* **2012**, *134*, 6104−6107.

(62) Bard, A. J.; Faulkner, L. R. In *Electrochemical Methods: Fundamentals and Applications*, 2nd ed.; Wiley: New York, 2001.

(63) Izutsu, K. *Acid-Base Dissociation Constants in Dipolar Aprotic Solvents*; Blackwell Science: Oxford, U.K., 1990.

(64) Roberts, J. A. S.; Bullock, R. M. *Inorg. Chem.* **2013**, *52*, 3823−3835.

(65) Fourmond, V.; Jacques, P.-A.; Fontecave, M.; Artero, V. *Inorg. Chem.* **2010**, *49*, 10338−10347.

(66) Appel, A. M.; Helm, M. L. *ACS Catal.* **2013**, *4*, 630−633.

(67) Bigi, J. P.; Hanna, T. E.; Harman, W. H.; Chang, A.; Chang, C. J. *Chem. Commun.* **2010**, *46*, 958−960.

(68) Stubbert, B. D.; Peters, J. C.; Gray, H. B. *J. Am. Chem. Soc.* **2011**, *133*, 18070−18073.

(69) McCrory, C. C. L.; Uyeda, C.; Peters, J. C. *J. Am. Chem. Soc.* **2012**, *134*, 3164−3170.

(70) Wilson, A. D.; Shoemaker, R. K.; Miedaner, A.; Muckerman, J. T.; DuBois, D. L.; DuBois, M. R. *Proc. Natl. Acad. Sci. U.S.A.* **2007**, *104*, 6951−6956.

(71) Andrieux, C. P.; Blocman, C.; Dumas-Bouchiat, J. M.; M'Halla, F.; Savéant, J.-M. *J. Electroanal. Chem.* **1980**, *113*, 19−40.

(72) Savéant, J.-M.; Su, K. B. *J. Electroanal. Chem.* **1984**, *171*, 341−349.

(73) Andrieux, C. P.; Dumas-Bouchiat, J. M.; Savéant, J. M. *J. Electroanal. Chem.* **1980**, *113*, 1−18.

(74) Savéant, J.-M. *Chem. Rev.* **2008**, *108*, 2348−2378.

(75) Kilgore, U. J.; Roberts, J. A. S.; Pool, D. H.; Appel, A. M.; Stewart, M. P.; DuBois, M. R.; Dougherty, W. G.; Kassel, W. S.; Bullock, R. M.; DuBois, D. L. *J. Am. Chem. Soc.* **2011**, *133*, 5861−5872.

(76) Dapporto, P.; Midollini, S.; Sacconi, L. *Inorg. Chem.* **1975**, *14*, 1643−1650.

(77) Lutz, F.; Bau, R.; Wu, P.; Koetzle, T. F.; Krueger, C.; Schneider, J. J. *Inorg. Chem.* **1996**, *35*, 2698−2700.

(78) Artero, V.; Chavarot-Kerlidou, M.; Fontecave, M. *Angew. Chem., Int. Ed.* **2011**, *50*, 7238−7266.

(79) Pangborn, A. B.; Giardello, M. A.; Grubbs, R. H.; Rosen, R. K.; Timmers, F. J. *Organometallics* **1996**, *15*, 1518−1520.

(80) *SAINT, Version 6.02*; Bruker AXS, Inc.: Madison, WI, 2001.

(81) *SADABS*; Bruker AXS, Inc.: Madison, WI, 2001.

(82) *SHELXTL Version 6.14*; Bruker AXS: Madison, WI, 2000.

(83) Sheldrick, G. *Acta Crystallogr., Sect. A* **2008**, *64*, 112−122.

7145

dx.doi.org/10.1021/ic500121f | *Inorg. Chem.* 2014, 53, 7137−7145